Cold magnetically trapped ^2D_g scandium atoms. I. Interaction potential

Tijs Karman,[1] Xi Chu,[2] and Gerrit C. Groenenboom[1,*]

[1]*Theoretical Chemistry, Institute for Molecules and Materials, Radboud University Nijmegen, Nijmegen, The Netherlands*

[2]*Department of Chemistry and Biochemistry, Center for Biomolecular Structure and Dynamics, University of Montana, Missoula, Montana 59812, USA*

(Received 27 July 2014; published 5 November 2014)

We present a first principles description of the interaction of two ground-state scandium atoms. Scandium has a ^2D_g ground state. Thirty molecular states correlate to the lowest dissociation limit of the dimer. In the short range, potential energy curves are calculated using second-order n-electron valence state perturbation theory. The first-order long-range interaction is calculated at the complete active space self-consistent field level. We determine the second-order long-range dispersion interaction from atomic dynamic polarizabilities at imaginary frequencies. These polarizabilities are calculated using time-dependent density functional theory. We merge the short-range approach with the long-range model to obtain a physical description of the 30 potential energy curves correlating to the $^2D_g + {}^2D_g$ limit. Diabatic potentials are presented that can be used in quantum scattering calculations, in order to study Zeeman relaxation of ultracold scandium atoms.

DOI: 10.1103/PhysRevA.90.052701 PACS number(s): 34.10.+x, 31.15.A−, 34.50.Cx

I. INTRODUCTION

Bose-Einstein condensates of atoms contained in magnetic traps are observed for mainly alkali metals [1–3]. These condensates are of interest, for example, to investigate the time variance of the fundamental constants [4–7], quantum many-body physics [8], and quantum computing [9,10]. Through techniques such as photoassociation [11] and Feshbach association [12], cold atoms are also of interest for the production of cold molecules. Evaporative cooling is a viable technique for the production of cold atoms if the rate of thermalizing elastic collisions is much larger than the rate of collisional reorientation of angular momentum, as this leads to trap loss [13].

Reorientation of the angular momenta of trapped atoms is driven by anisotropic interactions. The nonrelativistic electronic interaction of S-state atoms is isotropic, thus explaining the feasibility of evaporative cooling of light alkali atoms [1–3]. Anisotropic relativistic interactions may lead to large inelastic cross sections for heavier elements, e.g., for cesium [14]. For light open-shell atoms in states with orbital angular momentum $L > 0$, the anisotropy in the nonrelativistic electronic interaction is dominant. The interaction depends on the angles between the electronic angular momenta of both atoms and the internuclear axis, i.e., the potential energy depends on the electronic state of the dimer. Stated conversely, the interaction anisotropy lifts the degeneracy of the adiabatic electronic states of the dimer correlating to the ground-state atoms [15].

It has been proposed that interaction anisotropy may be suppressed for so-called submerged-shell atoms [16,17]. The open subshell of such atoms is shielded by a closed subshell of larger spatial extent. The partially filled subshell may contribute nonzero angular momentum, while the filled outer subshell renders the atom approximately spherically symmetric. Roughly a third of the elements possess such a structure, thus efficient cooling of such species would greatly increase the possibilities for forming quantum-degenerate gases.

The suppression of angular momentum changing collisions is seen to be efficient for scattering between helium and titanium [18–20], as well as for helium-erbium and helium-thulium collisions [21]. However, scattering of pairs of erbium or thulium atoms leads to unexpectedly large inelastic cross sections [21].

We consider scandium as a model system for submerged-shell atoms. The ground state of the scandium atom is a ^2D_g term, corresponding to an $[\mathrm{Ar}]4s^2 3d^1$ configuration. The filled $4s$ orbital has a much larger spatial extent than the orbitals of the $3d$ subshell, which qualifies the scandium atom as a submerged-shell atom. The interaction of two such atoms gives rise to 30 molecular states:

$$\begin{aligned}\mathrm{Sc}(^2D_g) + \mathrm{Sc}(^2D_g) \rightarrow \mathrm{Sc}_2\big(&{}^1\Sigma_g^+[3],\ {}^1\Sigma_u^-[2],\ {}^3\Sigma_g^-[2],\ {}^3\Sigma_u^+[3],\\ &{}^1\Pi_g[2],\ {}^1\Pi_u[2],\ {}^3\Pi_g[2],\ {}^3\Pi_u[2],\\ &{}^1\Delta_g[2],\ {}^1\Delta_u,\ {}^3\Delta_g,\ {}^3\Delta_u[2],\ {}^1\Phi_g,\\ &{}^1\Phi_u,\ {}^3\Phi_g,\ {}^3\Phi_u,\ {}^1\Gamma_g,\ {}^3\Gamma_u\big).\end{aligned} \tag{1}$$

An accurate first principles description of such a large number of states is a challenging task. The large spatial extent of the filled $4s$ subshell prevents covalent bonding. The bonding is therefore expected to be predominantly due to the dispersion interaction, making an accurate description of electronic correlation effects essential [22]. Moreover, the submerged-shell structure is thought to suppress the interaction anisotropy, leading to energetically closely spaced adiabatic states.

Most theoretical work on the scandium dimer has been concerned with its $X\,{}^5\Sigma_u^-$ electronic ground state [23,24]. This state correlates to a higher dissociation channel and is therefore less relevant for the description of cold atomic gases. Since the ground state is a quintet spin state, it is not coupled to the states studied in this work by the nonrelativistic electronic interaction. To our knowledge, the only study of the electronic states that correlate to the lowest dissociation channel are the multireference configuration interaction (MRCI) calculations by Kalemos *et al.* [22]. This method is not size-consistent, which leads to inaccuracy in the long-range regime.

*gerritg@theochem.ru.nl

The applicability of various multireference (MR) approaches to the electronic structure of transition metal dimers was assessed for manganese by Buchachenko *et al.* [25]. These methods are MR single and double excitation configuration interaction (MRCI), with Davidson correction for higher excitations (MRCI+Q), averaged quadratic coupled cluster (AQCC), and the second- and third-order perturbation theories: complete active space perturbation theory (CASPTn), n-electron valence state perturbation theory (NEVPTn), multiconfigurational quasidegenerate perturbation theory (MCQDPTn), and multireference Møller-Plesset perturbation theory (MRMPn), $n = 2,3$. Around the equilibrium geometry, perturbative methods with Fock-like zeroth-order Hamiltonians, such as CASPT2, are seen to be much less accurate than MRCI and related methods. Furthermore, such perturbation theories may be affected by the intruder-state problem [26]. More generally, it is concluded that all MR methods differ significantly from more accurate single-reference coupled-cluster calculations.

Unfortunately we must resort to MR methods for Sc_2, since none of the molecular states correlating to the $^2D_g + {}^2D_g$ limit are well described by a single determinant. In this paper we therefore employ the single-state NEVPT2 method [27–31]. This method was found to perform remarkably better than other perturbation theories, for the manganese dimer [25]. It provides a properly convergent perturbation expansion, as it is intruder-state free. Furthermore, the theory is formally size-consistent, although substantial deviations from size consistency have been observed in numerical studies [23]. In this paper, we report deviations from size consistency on the order of $10^{-3}E_h$. These deviations are not explained by symmetry breaking in the CASSCF wave function, but arise from numerical errors in the practical implementation of the NEVPT2 calculations.

Since the NEVPT2 calculations are insufficiently accurate to extract anisotropic long-range parameters, we determine the long-range interaction, in first- and second-order electrostatic perturbation theory [32]. The strength of the first-order electric quadrupole-quadrupole coupling is determined at the complete active space self-consistent field (CASSCF) level of theory. The second-order dispersion interaction is related to the dynamic polarizabilities of the atom. These are computed with time-dependent density functional theory (TD-DFT) [33,34]. Finally, short-range potentials are calculated at the NEVPT2 level of theory. This results in physically acceptable global PECs for all 30 molecular states correlating to the lowest dissociation limit. Predicted spectroscopic parameters are in reasonable agreement with earlier MRCI calculations [22].

In this paper we present diabatic potentials, in addition to the adiabatic PECs. These diabatic potentials are employed in quantum scattering calculations in the companion paper [35]. As pointed out in Ref. [36], describing the collision of open-shell atoms in an adiabatic basis leads to angular nonadiabatic couplings that vanish only as $1/R$. That is, the nonadiabatic coupling vanishes much more slowly than the energy splitting due to the long-ranged quadrupole-quadrupole interaction, $\propto R^{-5}$, and the asymptotic scattering boundary conditions must be modified in order to account for the nonadiabatic coupling. To avoid these difficulties, it is essential that the nonadiabatic couplings are eliminated by employing a diabatic basis of space-fixed atomic states [36]. We use the diabatic model proposed in Ref. [15] in order to relate diabatic potentials to the Born-Oppenheimer potentials, which are calculated in this paper. This theory has previously been applied to the collision of P-state atoms [37–39]. The interaction of P-state atoms can be considered a special case, since each adiabatic state of the dimer can be assigned definite asymptotic total electronic orbital angular momentum. For $L \geqslant 2$ state atoms, this is no longer the case, and in that sense, the present work can be considered the first application of the general theory of Ref. [15]. To the best of our knowledge, only model potentials exist for interacting $L \geqslant 2$ state atoms [40].

This article is organized as follows. In Sec. II we discuss the space-fixed tensorial expansion of the interaction potential, the relation of the expansion coefficients to the PECs of the dimer, and multipole expansion of the interaction [15]. In Sec. III the supermolecular approach is discussed, where we emphasize on the long-range potential. Section IV describes the TD-DFT calculation of the dynamic polarizabilities of the atom, from which the long-range dispersion interaction is calculated. Section V discusses how the PECs were fit and merged with the long-ranged model. Concluding remarks are given in Sec. VI.

II. THEORY

A. Tensorial expansion of the interaction

To describe the interaction of two open-shell atoms, we adopt the irreducible spherical tensor formalism and notation introduced in Refs. [15,32]. The Russel-Saunders coupled atomic state of atom A is written as $|L_A M_A\rangle|S_A \Sigma_A\rangle$, where the angular momentum ket $|L_A M_A\rangle$ describes the electronic orbital degrees of freedom in the space-fixed frame, and $|S_A \Sigma_A\rangle$ describes the electron spin. Since scandium is a ^2D_g state atom, we have $L_A = 2$ and $S_A = 1/2$. The interaction of two such atoms may be expanded in unit irreducible spherical tensor operators, defined by

$$T_{kq}(L) \equiv \sum_{M,M'} |LM\rangle\langle LM'|(-1)^{L-M} \begin{pmatrix} L & k & L \\ -M & q & M' \end{pmatrix} [k]^{1/2}. \tag{2}$$

Here the symbol in round brackets is a 3-jm symbol, and $[k]$ is a short-hand notation for $2k + 1$. The interaction potential is given by the space-fixed expansion:

$$\begin{aligned} \hat{V} &= \sum_{S,\Sigma} |S\Sigma\rangle\langle S\Sigma|\hat{V}^{(S)}, \\ \hat{V}^{(S)} &= \sum_{k_A,k_B,k_{AB}} V^{(S)}_{k_A k_B k_{AB}}(R) \\ &\quad \times \sum_{q_{AB}} [\hat{T}_{k_A}(L_A) \otimes \hat{T}_{k_B}(L_B)]^{(k_{AB})}_{q_{AB}} C^*_{k_{AB} q_{AB}}(\hat{\boldsymbol{R}}). \end{aligned} \tag{3}$$

The symbol C_{kq} denotes a Racah normalized spherical harmonic, $\hat{\boldsymbol{R}}$ denotes the polar angles of the internuclear axis, and R is the internuclear distance. The symbol

$$\begin{aligned} &[\hat{T}_{k_A}(L_A) \otimes \hat{T}_{k_B}(L_B)]^{(k)}_q \\ &\quad = \sum_{q_A,q_B} \hat{T}_{k_A q_A}(L_A)\hat{T}_{k_B q_B}(L_B)\langle k_A q_A k_B q_B|kq\rangle \end{aligned} \tag{4}$$

is the spherical component q of the irreducible rank-k tensor product of $\hat{T}_{k_A}(L_A)$ and $\hat{T}_{k_B}(L_B)$. The symbol $\langle k_A q_A k_B q_B | k q\rangle$ denotes a Clebsch-Gordan coefficient. In Eq. (3), the sum over k_A runs from 0 to $2L_A$, the sum over k_B runs from 0 to $2L_B$, and the sum over k is restricted to even values for which $|k_A - k_B| \leqslant k_{AB} \leqslant k_A + k_B$. The term with $k_A = k_B = k_{AB} = 0$ is the isotropic potential, whereas other terms represent the anisotropic components of the interaction.

Using the diabatic model of Ref. [15], the expansion coefficients $V^{(S)}_{k_A k_B k}(R)$ are related to the Born-Oppenheimer potentials of the supermolecule, i.e., the dimer, by

$$V^{(S)}_{k_A k_B k_{AB}}(R) = \sum_{c,\Lambda,L,L'} V_{c\Lambda S}(R) U^{\Lambda *}_{L,c} U^{\Lambda}_{L',c} (-1)^{L-\Lambda} [k_A, k_B, k_{AB}, L, L']^{1/2} \times \begin{pmatrix} L & k_{AB} & L' \\ -\Lambda & 0 & \Lambda \end{pmatrix} \begin{Bmatrix} L_A & L_A & k_A \\ L_B & L_B & k_B \\ L & L' & k_{AB} \end{Bmatrix}. \quad (5)$$

The sums over L and L' run from $|L_A - L_B|$ to $L_A + L_B$, the sum over Λ runs from $-\min(L, L')$ to $\min(L, L')$, and c enumerates the adiabatic states. The symbol in curly braces represents a 9-j symbol, $V_{c\Lambda S}(R)$ are the adiabatic potentials of the dimer, and $U^{\Lambda}_{L,c}$ is an element of the unitary transformation that diagonalizes the quadrupole-quadrupole interaction in the space of coupled atomic states in the body-fixed frame, defined by

$$|(L_A L_B) L \Lambda\rangle = \sum_{\Lambda_A, \Lambda_B} |L_A \Lambda_A\rangle |L_B \Lambda_B\rangle \langle L_A \Lambda_A L_B \Lambda_B | L \Lambda\rangle. \quad (6)$$

See the Appendix for a detailed discussion of the diagonalization of the quadrupole-quadrupole interaction, albeit in a different basis. This diabatic representation eliminates angular nonadiabatic coupling, varying asymptotically with $1/R$ [15,36]. This is essential for the application of the potential in scattering calculations.

B. Long-range theory

In the long range, the interaction can be described using degenerate perturbation theory and expanded as a power series in R^{-1} [32]. In absence of exchange, the interaction becomes independent of spin, and the expansion coefficients are

$$V^{(S)}_{k_A k_B k_{AB}}(R) = \sum_n \frac{c_{n,(k_A k_B) k_{AB}}}{R^n}. \quad (7)$$

If we consider first- and second-order interactions only, we have

$$c_{n,(k_A k_B) k_{AB}} = c^{(1)}_{n,(k_A k_B) k_{AB}} - c^{(2)}_{n,(k_A k_B) k_{AB}}, \quad (8)$$

where the minus sign in front of the second-order coefficient, $c^{(2)}_{n,(k_A k_B) k_{AB}}$, is conventional. The first-order coefficients, $c^{(1)}_{n,(k_A k_B) K_{12}}$, are nonzero for even $k_A \leqslant 2L_A$ and $k_B \leqslant 2L_B$, with $K_{12} = k_A + k_B$ and $n = K_{12} + 1$. They are given by

$$c^{(1)}_{n,(k_A k_B) K_{12}} = (-1)^{k_B} \begin{pmatrix} 2K_{12} \\ 2k_B \end{pmatrix}^{1/2} Q^{(A)}_{k_A}(L_A) Q^{(B)}_{k_B}(L_B), \quad (9)$$

where the symbol in parentheses is a binomial coefficient, and $Q^{(A)}_{k_A}(L_A)$ is the reduced matrix element of a multipole operator of atom A. The Wigner-Eckart theorem relates the atomic multipole moments to the reduced matrix elements through

$$\langle L_A M_A | \hat{Q}^{(A)}_{kq} | L_A M'_A \rangle = (-1)^{L_A - M_A} [k]^{1/2} \begin{pmatrix} L_A & k & L_A \\ -M_A & q & M'_A \end{pmatrix} Q^{(A)}_k(L_A). \quad (10)$$

The multipole operators of atom A are defined by

$$\hat{Q}^{(A)}_{kq} = \sum_i q_i r_i^k C_{kq}(\boldsymbol{r}_i), \quad (11)$$

where the sum is over all particles, i, with charge q_i, and position $\boldsymbol{r}_i$, which is measured with respect to the position of nucleus A, $\boldsymbol{R}_A$. Similar equations hold for atom B. We will only consider the leading term, which is the quadrupole-quadrupole interaction ($k_A = k_B = 2$).

At second order, we will consider dipole-dipole dispersion contributions only. The dispersion interaction coefficients are related to the reduced matrix elements of the dynamic polarizabilities of the atoms at imaginary frequencies $\alpha^{(A)}_{(l_A l'_A) k_A}(L_A; i\omega)$ through

$$c^{(2)}_{n,(k_A k_B) k} = \sum_{l_A l_B l'_A l'_B} \frac{f^{(k_A k_B k)}_{l_A l_B l'_A l'_B}}{2\pi} \int_0^\infty \alpha^{(A)}_{(l_A l'_A) k_A}(L_A; i\omega) \times \alpha^{(B)}_{(l_B l'_B) k_B}(L_B; i\omega) d\omega, \quad (12)$$

where $n = l_A + l'_A + l_B + l'_B + 2$ and $k_A + k_B$ and k must be even. The coefficients $f^{(k_A k_B k)}_{l_A l_B l'_A l'_B}$ are given by Eq. (21) in Ref. [32]. In Table I we tabulate them for dipole-dipole terms ($l_A = l'_A = l_B = l'_B = 1$).

For each atomic state $|LM\rangle$ with energy E_L, we define the dynamic dipole-dipole polarizability at imaginary frequency

$$\alpha_u(LM; i\omega) = 2 \sum_{\gamma M_\gamma} \frac{(E_\gamma - E_L) |\langle \gamma L_\gamma M_\gamma | \hat{\mu}_u | LM\rangle|^2}{(E_\gamma - E_L)^2 + \omega^2}. \quad (13)$$

Here $\hat{\mu}_u$ are the Cartesian ($u = x, y, z$) or spherical ($u = 0, +1, -1$) space-fixed components of the dipole operator, and the sum is over all excited states $|\gamma L_\gamma M_\gamma\rangle$, with energy E_γ. We also use the notation $\hat{\mu}_\parallel = \hat{\mu}_z = \hat{\mu}_0$. The $\pm$ spherical components of the dipole operator are given by $\hat{\mu}_\pm = \mp(\hat{\mu}_x \pm i\hat{\mu}_y)/\sqrt{2}$. The sum of the ± 1 spherical components of the polarizability is related to the perpendicular component

TABLE I. The coefficients $f^{(k_A, k_B, k)}_{1,1,1,1}$ for dipole-dipole dispersion.

k_A	k_B	k	$f^{(k_A,k_B,k)}_{1,1,1,1}$
0	0	0	2
1	1	0	$-\sqrt{3}$
2	2	0	$\sqrt{1/5}$
1	1	2	$-\sqrt{6}$
0	2	2	$-\sqrt{2}$
2	0	2	$-\sqrt{2}$
2	2	2	$\sqrt{2/7}$
2	2	4	$18\sqrt{2/35}$

through

$$\alpha_{\perp}(LM) = \frac{\alpha_{+1}(LM) + \alpha_{-1}(LM)}{2}, \tag{14}$$

where we dropped the ω dependence for compactness. In the notation of Ref. [32] we have

$$\begin{aligned} \alpha_{\parallel}(LM) &= \alpha^{+}_{1,0;1,0}(LM), \\ \alpha_{\perp}(LM) &= -\alpha^{+}_{1,1;1,-1}(LM). \end{aligned} \tag{15}$$

With use of Eqs. (8) and (9) of Ref. [41], the polarizabilities $\alpha_{\parallel}(LM)$ and $\alpha_{\perp}(LM)$ can be expressed in terms of the scalar polarizability, $\alpha_0(LM)$, and the rank-2 tensor polarizability, $\alpha_2(LM)$, as

$$\begin{aligned} \alpha_{\parallel}(L,M) &= \alpha_0(L) + \alpha_2(L)\frac{3M^2 - L(L+1)}{L(2L-1)}, \\ \alpha_{\perp}(L,M) &= \alpha_0(L) - \frac{1}{2}\alpha_2(L)\frac{3M^2 - L(L+1)}{L(2L-1)}. \end{aligned} \tag{16}$$

These equations show that $\alpha_0(L)$ and $\alpha_2(L)$ may in principle be determined from $\alpha_{\perp}(L,M)$ and $\alpha_{\parallel}(L,M)$ of a single magnetic substate. Alternatively, one may determine the $\alpha_0(L)$ and $\alpha_2(L)$ from a linear least squares fit to the polarizabilities of multiple substates, and use the deviation from Eq. (16) to validate the internal consistency of the method. By comparing Eq. (16) to Eq. (41) of Ref. [32], we derive

$$\alpha_{(1,1)0}(L) = -\sqrt{3(2L+1)}\alpha_0(L) \tag{17}$$

and

$$\alpha_{(1,1)2}(L) = \left[\frac{3(L+1)(2L+1)(2L+3)}{10L(2L-1)}\right]^{1/2}\alpha_2(L). \tag{18}$$

The difference of the ± 1 spherical components of the dipole-dipole polarizability can be written in the notation of Ref. [32] as

$$\alpha^{-}_{1,1;1,-1}(L,M) = \frac{\alpha_{-1}(L,M) - \alpha_{+1}(L,M)}{2}. \tag{19}$$

Equation (42) of Ref. [32], in the dipole-dipole case, becomes

$$\alpha^{-}_{1,1;1,-1}(L,M) = M\left[\frac{3}{2L(L+1)(2L+1)}\right]^{1/2}\alpha_{(1,1)1}(L). \tag{20}$$

Hence, when $M \neq 0$ we can use this expression to find the rank-1 reduced dipole-dipole polarizability $\alpha_{(1,1)1}(L)$. These are known as out-of-phase polarizabilities, and they play no role for the interaction with rare gas atoms [32]. We are not aware of previous calculations of the out-of-phase polarizability of open-shell atoms.

III. SUPERMOLECULAR APPROACH

A. Computational method

All supermolecular calculations have been carried out in the augmented correlation consistent basis set of quadruple cardinality, aug-cc-pVQZ [42]. Molecular orbitals have been generated with the MCSCF program [43–47] of the MOLPRO package [48,49] by performing state-averaged CASSCF calculations. The active space contains six electrons in symmetry adapted combinations of the $4s$ and $3d$ valence, and the $4p$ virtual atomic orbitals. This choice of active space, termed full valence CAS, was found preferable in earlier work on transition metal dimers [23,25]. Subsequently, single-state NEVPT2 calculations were performed.

In the short range, calculations were performed using an equally spaced radial grid, ranging from 5.9 to 8.5 a_0, with a grid spacing of 0.2 a_0. In the long range, we use a logarithmically spaced grid, consisting of the points 9.0357, 9.6052, 10.2106, 10.8541, 11.5382, 12.2654, 13.0384, 13.8602, 14.7337, 15.6623, 16.6494, 17.6988, and 18.8142 a_0.

B. Counterpoise procedure

Interaction energies which are obtained by the super-molecular approach always contain the basis set superposition error (BSSE) [50]. This error can be reduced by subtracting the energy of the individual atoms, evaluated in the same one-electron basis as used in the super-molecular calculation, rather than subtracting the energy of two well separated atoms. For closed-shell fragments, this procedure is known as the counterpoise procedure of Boys and Bernardi [51].

For fragments in degenerate open-shell states, a generalized counterpoise procedure is more involved. Alexander proposed to calculate BSSE-corrected interaction energies in a diabatic representation, for the $B(^2P) - H_2$ system [52]. Kłos *et al.* were the first to propose a generalized counterpoise procedure for the adiabatic states of systems involving an open-shell fragment [53].

When this procedure is applied to systems consisting of one $L > 0$ atom and one rare gas atom, one encounters the issue that the calculated monomer energy depends on the Λ quantum number, in addition to the geometry of the complex [54]. In this case, a generalized counterpoise procedure can be constructed by subtracting monomer energies, calculated with the same value of Λ as the molecular state.

For systems dissociating to two $L > 0$ atoms, the situation is slightly more complicated, as multiple atomic substates contribute to a single molecular state. We use a generalized counterpoise procedure [55], which estimates the monomer energy for a given state as the weighted average of the energies of atomic substates, evaluated in the dimer basis. The weights of this average are estimated from the contribution to the asymptotic wave function. See the Appendix for additional details on how the asymptotic wave functions are determined.

C. Size consistency

From theoretical considerations, the NEVPT2 method is known to be size-consistent. In numerical studies, however, appreciable errors in size consistency are observed. Camacho *et al.* [23] report an estimated 1 mE_h error in size consistency, for the electronic ground state of Sc_2. Such an error may be considered small when studying the equilibrium properties of covalently bound states, but it is quite large compared to the weak dispersion interaction, studied in this work.

We estimate the deviation from size consistency of the NEVPT2 calculations for the studied states near $R = 20$ a_0 to be on the order of 1 mE_h, consistent with the findings of Camacho *et al.* [23]. They attribute this error to symmetry

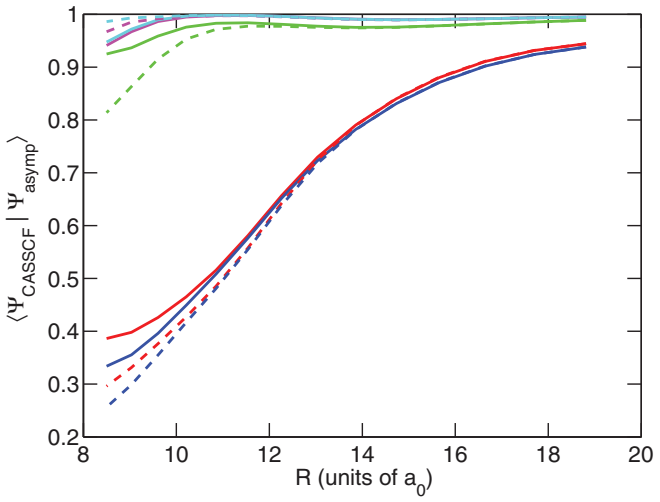

FIG. 1. (Color online) Scalar product of CASSCF and theoretical asymptotic wave functions, as a function of the internuclear distance. Solid lines correspond to singlet states, dashed lines represent triplet states. Green, red, and blue lines correspond to the Σ^+ states, ordered by increasing energy. The magenta and cyan lines correspond to the Σ^- states.

breaking of the underlying CASSCF calculation [23]. However, for the CASSCF calculations we performed, we estimated the deviation from size consistency to be close to the energy convergence criterion that is used. This does not support the hypothesis that symmetry breaking of the underlying CASSCF calculation is responsible for the lack of size consistency of the NEVPT2 calculations.

To obtain a physical description of the long-range interaction, the condition that the interaction vanishes at infinite separation might not be sufficient. As a more stringent test of the size consistency of the state-averaged CASSCF procedure, we compared the numerical wave functions to the theoretical asymptotic form [32]. We conclude that the zeroth-order wave functions approach the theoretical limit smoothly, which is illustrated in Fig. 1 for the 10 Σ states. This figure shows the scalar product of the CASSCF states and the corresponding theoretical limits, as a function of the internuclear distance, R. A detailed description of how this result was obtained is given in the Appendix.

D. Numerical results

We obtained PECs at the NEVPT2 level for all 30 molecular states correlating to the $Sc(^2D_g) + Sc(^2D_g)$ limit. The *ab initio* points are shown as the dots in Fig. 2, and the solid lines show a fit to the potentials, which is discussed in Sec. V. It appears from Fig. 2 that additional calculations at shorter R are required, as we have not yet reached the repulsive regime for all states. However, at shorter separation, the state-averaged CASSCF procedure does not converge, and we have performed additional single-state calculations at shorter separation. In Sec. V we conclude that with this extension we obtain almost identical fits. Thus, we leave out this extension for simplicity, such that we do not have to merge the single-state and state-averaged approaches.

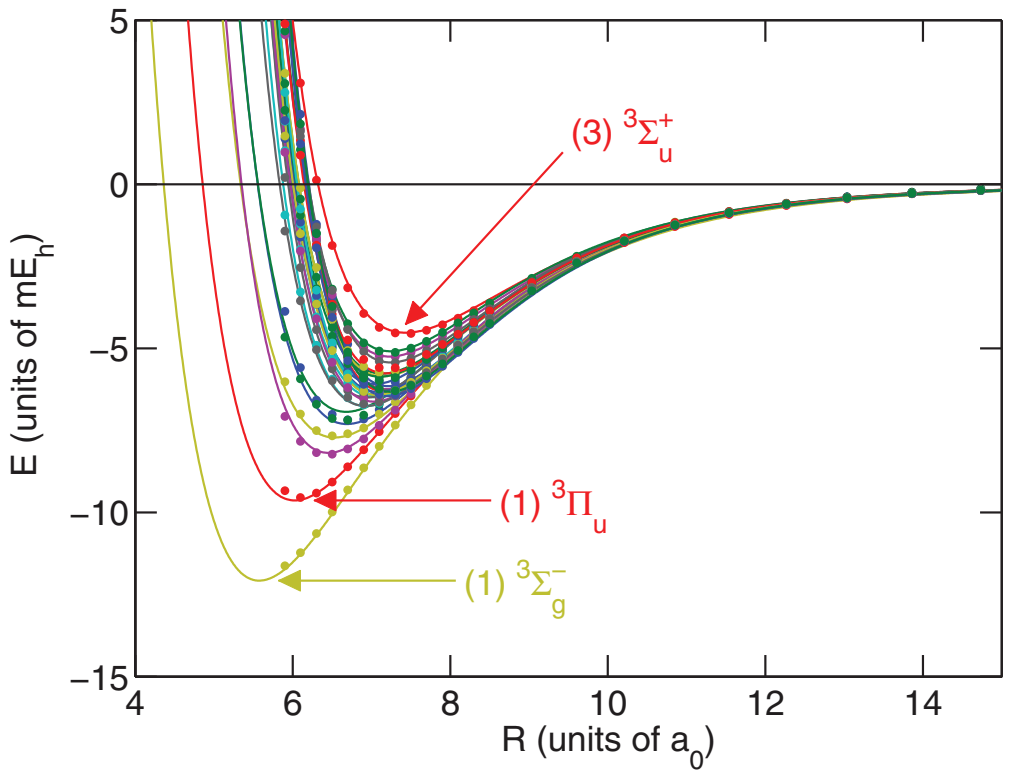

FIG. 2. (Color online) Adiabatic PECs for all 30 molecular states studied, calculated using the NEVPT2 method. Dots denote *ab initio* points, and solid lines denote the anaytical fit discussed in Sec. V. Spectroscopic parameters for all 30 states are given in Table V.

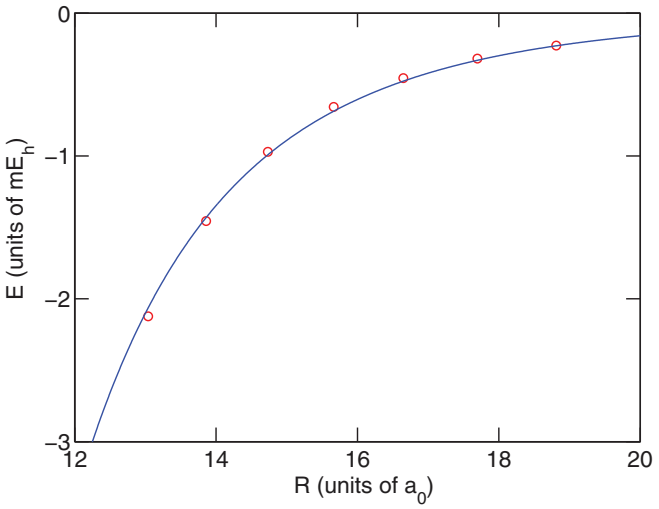

FIG. 3. (Color online) Space-fixed expansion coefficient $V_{000}(R)$, vertically shifted *ab initio* points at the NEVPT2 level of theory are marked with red circles, and the R^6 weighted fit is represented by the blue line.

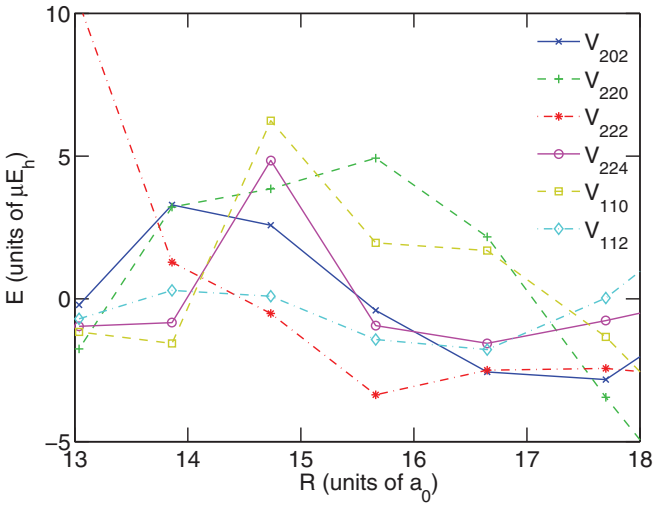

FIG. 4. (Color online) Vertically shifted space-fixed expansion coefficients corresponding to anisotropic long-range interactions at the NEVPT2 level of theory.

The diabatic representation of Ref. [15] diabatizes angular nonadiabatic coupling. Radial nonadiabatic couplings may also exist. In particular, an avoided crossing of the second and third state of $^1\Sigma_g^+$ symmetry near $R = 7.3\ a_0$ we observed. The first and second state of $^3\Sigma_u^+$ symmetry show an avoided crossing near $R = 6.8\ a_0$. An upper bound to the off-diagonal element of the diabatic potential can be found by inspecting the splitting of the adiabatic states near the crossing. We did not attempt to locate the crossings exactly but used the radial grid specified before. We found that the coupling is smaller than $10^{-4}E_h$ and $10^{-7}E_h$ for the singlet and triplet states, respectively. Since these crossings occur near the minimum of the potential well, the couplings are small when compared to the local nuclear kinetic energy. Thus, we were able to approximately diabatize the crossings by neglecting this coupling and switching the *ab initio* points at shorter separation [56].

Next, we obtain the coefficients, $V_{k_Ak_Bk_{AB}}(R)$, of the space-fixed tensorial expansion using Eq. (5). We are able to obtain the isotropic parameter $c^{(2)}_{6,(00)0}$ from a R^6 weighted linear least squares fit to $V_{000}(R)$. This yields $c^{(2)}_{6,(00)0} = 10145.16\ E_h a_0^6$. In obtaining this fit, we allowed for a shift of the potential energy curves, in order to account for the error in size consistency. The fit is shown in Fig. 3.

The anisotropic dispersion and quadrupole-quadrupole parameters could not be resolved from the computed PECs at the NEVPT2 level of theory. Coefficients $V_{k_Ak_Bk_{AB}}(R)$ containing contributions from first-order quadrupole-quadrupole coupling and second-order dipole-dipole dispersion are seen not to vary with R^{-5} and R^{-6}, respectively. This is illustrated in Fig. 4. Remaining expansion coefficients should be negligible compared to the terms shown in Fig. 4; however, they are found to be comparable.

As shown, the CASSCF method offers a physically acceptable description of the long-range wave function. The limited treatment of electron correlation at this level of theory, however, does not allow for a proper description of the dispersion interaction. Still, the first-order quadrupole-quadrupole coupling should be well described at this level of theory. The corresponding coefficient, $c^{(1)}_{5,(22)4}$, is determined from a R^5 weighted linear fit, which is shown in Fig. 5. This way, we obtained the value $c^{(1)}_{5,(22)4} = 25.67\ E_h a_0^5$, without having to correct for a size inconsistency, which is absent for the CASSCF calculations.

Using Eq. (9), the first-order coefficient can be related to the square of the reduced quadrupole moment. The coefficient extracted from the CASSCF PECs implies $|\langle 20|\Theta_{zz}|20\rangle| = 0.94$ a.u. This is in reasonable agreement with the quadrupole moment $\langle 20|\Theta_{zz}|20\rangle = -1.04$ a.u. obtained by Kłos as the expectation value of the quadrupole moment in CASSCF calculations for the scandium atom, using a different basis set [57].

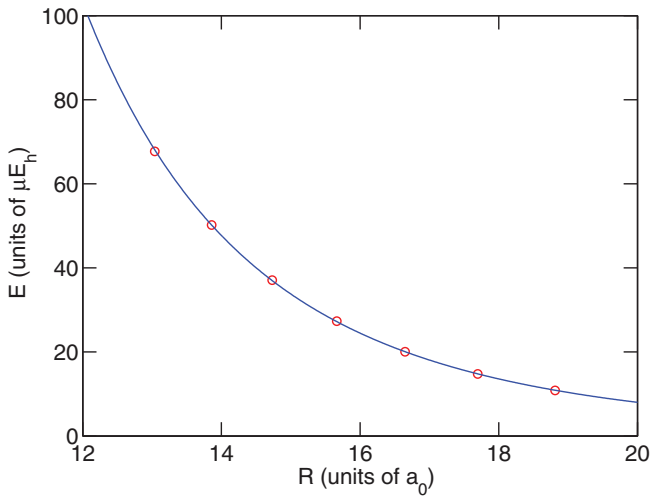

FIG. 5. (Color online) Space-fixed expansion coefficient $V_{224}(R)$, *ab initio* points at the CASSCF level of theory are marked with red circles, and the R^5 weighted fit is represented by the blue line.

Since we are unable to extract anisotropic dispersion coefficients from the PECs, we determine them from the dynamic polarizabilities of the atoms. The computation of these polarizabilities is presented in the following section.

IV. DYNAMIC POLARIZABILITIES

A. Computational method

The dynamic polarizabilities of scandium are determined using linear response TD-DFT. A detailed description of the method is given in Refs. [33,34]. The method has provided polarizabilities to within an uncertainty of about 5%. Furthermore, the method becomes exact in the limit of high frequencies. We used the local spin density approximation with self-interaction correction [33]. This functional gives the correct $-1/r$ long-range potential, which is important for the description of electronically excited states and the continuum, and hence for determining the polarizability.

B. Results

Figure 6 shows the frequency-dependent polarizabilities $\alpha_\perp(LM;i\omega)$ for the magnetic substates with $M = 1$ and $M = 2$. The solid lines correspond to the values obtained from Eq. (16), with the scalar (α_0) and tensor (α_2) polarizabilities taken from Ref. [41]. The dashed lines represent the values obtained as the average of the spherical components, Eq. (14). At $\omega = 0$ the two methods are in good agreement. For $\omega > 0$ we assume that the values obtained from α_0 and α_2 of Ref. [41] are more reliable.

The rank-1 polarizability $\alpha^-_{(1,1)1}(L;i\omega)$ can be computed from the spherical components of any substate with $M \neq 0$ with Eqs. (19) and (20). Figure 7 shows the rank-1 polarizability computed from the $M = 1$ and $M = 2$ substates. Clearly, the agreement between the results derived from the different substates is not quantitative. However, we may conclude that the rank-1 polarizability is small, which is probably at least part of the reason why it is difficult to obtain fully converged results.

From these polarizabilities, dispersion coefficients were determined using Eq. (12). They are given in Table II. This table also shows results obtained from the polarizabilities of titanium, determined in a similar calculation. This allows us to determine dispersion coefficients for the systems Sc − Sc, Sc − Ti, and Ti − Ti. The anisotropic dispersion coefficients for these systems are in the same order of magnitude. This motivates the study of the Sc − Sc system as a model for submerged-shell atoms and illustrates that our calculations have at least qualitative meaning for other submerged-shell systems.

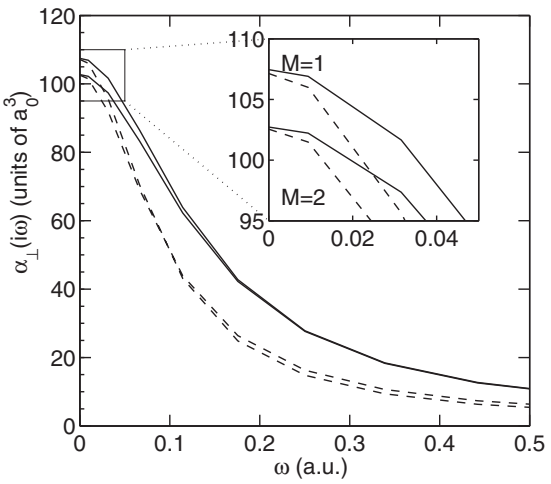

FIG. 6. The perpendicular polarizability at imaginary frequencies.

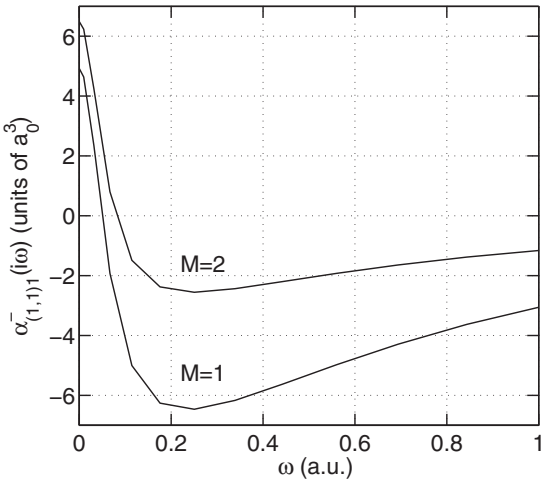

FIG. 7. The out-of-phase polarizability at imaginary frequencies, computed from different magnetic substates.

Combining the dispersion coefficients from Table II with the quadrupole-quadrupole coupling at the CASSCF level, and short-range effects calculated at the NEVPT2 level yields physically acceptable global PECs. The analytical representation of these PECs is discussed in the following section.

V. ANALYTICAL REPRESENTATION

We represent the adiabatic potentials by the functional form

$$V(R) = V_{\rm SR} + V_{\rm LR}(R),$$
$$V_{\rm SR}(R) = Ae^{-\alpha R} + Be^{-2\alpha R}, \qquad (21)$$

TABLE II. Dispersion coefficients $c^{(2)}_{6,(k_A k_B)k}$ in units of $E_h a_0^6$ calculated from the dynamic polarizabilities at imaginary frequency. Results are shown for the systems Sc − Sc, Sc − Ti, and Ti − Ti.

k_A	k_B	k	Sc − Sc	Sc − Ti	Ti − Ti
0	0	0	6108.40	6678.07	7314.79
2	2	0	1.01	0.65	0.39
0	2	2	108.99	117.67	73.08
2	0	2	108.99	67.68	73.08
2	2	2	1.21	0.77	0.46
2	2	4	9.75	6.03	3.71
1	1	0	−1.49[a]	−1.06[a]	−0.84[a]
			−8.00[b]	−10.06[b]	−13.02[b]
1	1	2	−2.11[a]	−1.54[a]	−1.19[a]
			−11.35[b]	−14.2[b]	−18.41[b]

[a]Computed from polarizabilities of the $M = 2$ substate for Sc and $M = 3$ for Ti.

[b]Computed from polarizabilities of the $M = 1$ substate for Sc and $M = 2$ for Ti.

with R the internuclear distance, A, B, and α constants and V_{LR} the damped long-range potential. The long-range potential is obtained by diagonalizing the interaction matrix, Eq. (3), where the expansion coefficients, $V^{(S)}_{k_A,k_B,k_{AB}}(R)$ are given by their long-range form, Eq. (7). Prior to diagonalization, the long-range interaction is damped by multiplying with Tang-Toennies functions [58] of the form

$$f_{n,\beta_n}(R) = 1 - e^{-\beta_n R} \sum_{k=0}^{n} \frac{(\beta_n R)^k}{k!}. \tag{22}$$

The long-range quadrupole-quadrupole contributions are damped by Tang-Toennies functions with $n = 5$, whereas we use $n = 6$ for the dispersion. The damping parameter for dispersion contributions, β_6, has been determined by minimizing the difference between the damped isotropic dispersion and the isotropic part of the *ab initio* potential between 7.5 and 13 a_0. The isotropic part of the *ab initio* potential is obtained by averaging the potential over all adiabatic states. The damping parameter for the quadrupole-quadrupole interaction, β_5, has been chosen such that both damping functions fall off in the same region. This procedure yields $\beta_6 = 0.9464\ a_0^{-1}$ and $\beta_5 = 0.8097\ a_0^{-1}$. The Morse parameters α, A, and B are then used as free parameters in a fit, to reproduce the *ab initio* data.

As described, the first-order coefficient $c^{(1)}_{5,(22)4}$ was determined in a linear fit to the CASSCF potentials, whereas the anisotropic dispersion coefficients were determined from the dynamic polarizabilities at the TD-DFT level of theory. The isotropic long-range parameter $c^{(2)}_{6,(00)0}$ could be determined both from the PECs at the NEVPT2 level of theory, and from the dynamic polarizabilities. The value obtained from the PECs is about 1.66 times as large as the one determined from the polarizabilities. In order to obtain a smooth fit, we use the isotropic dispersion parameter extracted from the *ab initio* curves. Furthermore, we use the dispersion coefficients determined from out-of-phase polarizabilities for the magnetic substate with $M = 2$. The resulting long-range parameters are summarized in Table III.

The obtained Morse parameters for all adiabatic states are given in Table IV. The fit adiabats are shown as the solid curves in Fig. 2. At shorter separation, the state-averaged CASSCF calculation does not converge. However, we were able to converge single-state CASSCF calculations at smaller separation. After merging the two methods, however, the fitting procedure yields almost identical Morse parameters.

TABLE III. Long-range parameters as used in the fit.

n	k_A	k_B	k	$c_{n,(k_A k_B)k}$ (units of $E_h a_0^n$)
5	2	2	4	25.67
6	0	0	0	10145.16
6	1	1	0	− 1.49
6	2	2	0	1.01
6	0	2	2	108.99
6	2	0	2	108.99
6	1	1	2	− 2.11
6	2	2	2	1.21
6	2	2	4	9.75

TABLE IV. Morse parameters as defined in Eq. (21).

	α (units of a_0^{-1})	A (units of E_h)	B (units of E_h)
$(1)^1\Sigma_g^+$	0.6429	− 0.2191	32.3323
$(2)^1\Sigma_g^+$	0.6518	− 0.2013	33.5686
$(3)^1\Sigma_g^+$	0.7808	− 0.8232	301.0327
$(1)^1\Sigma_u^-$	0.6817	− 0.3696	74.0516
$(2)^1\Sigma_u^-$	0.7590	− 0.7201	236.4561
$(1)^3\Sigma_g^-$	0.5692	− 0.1078	6.6462
$(2)^3\Sigma_g^-$	0.7309	− 0.6618	170.7965
$(1)^3\Sigma_u^+$	0.7615	− 0.6261	242.0053
$(2)^3\Sigma_u^+$	0.7144	− 0.3616	109.8344
$(3)^3\Sigma_u^+$	0.6650	− 0.2298	68.6506
$(1)^1\Pi_g$	0.7181	− 0.4401	118.8352
$(2)^1\Pi_g$	0.7069	− 0.2795	102.0495
$(1)^1\Pi_u$	0.5903	− 0.1712	15.9132
$(2)^1\Pi_u$	0.7785	− 0.4653	202.8802
$(1)^3\Pi_g$	0.7100	− 0.4053	106.6118
$(2)^3\Pi_g$	0.7127	− 0.2463	107.0224
$(1)^3\Pi_u$	0.6080	− 0.1220	12.7839
$(2)^3\Pi_u$	0.7191	− 0.4327	102.5326
$(1)^1\Delta_g$	0.6723	− 0.2004	36.1782
$(2)^1\Delta_g$	0.7068	− 0.3728	102.8320
$(1)^1\Delta_u$	0.7406	− 0.2931	160.8453
$(1)^3\Delta_g$	0.7281	− 0.2843	115.8887
$(1)^3\Delta_u$	0.7193	− 0.2841	110.3949
$(2)^3\Delta_u$	0.7339	− 0.4246	149.4404
$(1)^1\Phi_g$	0.7273	− 0.4478	135.8398
$(1)^1\Phi_u$	0.7059	− 0.4499	99.4057
$(1)^3\Phi_g$	0.7048	− 0.4305	99.7953
$(1)^3\Phi_u$	0.6810	− 0.2993	63.3394
$(1)^1\Gamma_g$	0.7283	− 0.6539	167.1227
$(1)^3\Gamma_u$	0.7322	− 0.6547	178.6433

For simplicity, we therefore use the fit to the PECs based on the state-averaged calculations, thereby avoiding having to merge the two procedures. The calculations with single-state CASSCF reference functions are considered a check on the repulsive part of the potentials.

The short range of the potential is characterized by spectroscopic constants, of which the equilibrium distance, R_e, well depth, D_e, and harmonic frequency, ω_e, are listed in Table V. For comparison, this table also includes the results of Kalemos *et al.* [22] at the MRCI/cc-pVQZ level of theory. Experimental data are not yet available for the studied states. The difference (root mean square error) between the calculated dissociation energies is 8.8%, harmonic frequencies agree within 8.4%, and the bond length within 5.2%. Notably, the bond lengths are consistently shorter at the NEVPT2 level of theory. This is in agreement with the findings of Buchachenko *et al.* [25], who found perturbation approaches generally give too short bond lengths and overestimate the well depth for transition metal dimers.

VI. CONCLUSION

We present global PECs for the 30 molecular states correlating to the lowest dissociation channel of the scandium dimer. Short-range effects are calculated using NEVPT2 in an augmented basis set of quadruple cardinality. A deviation from

TABLE V. Spectroscopic constants for the 30 molecular states that correlate to the lowest dissociation channel, as calculated at the NEVPT2/aug-cc-pVQZ level of theory in the present work and MRCI/cc-pVQZ of Ref. [22].

	NEVPT2			MRCI		
	D_e (units of mE_h)	R_e (units of a_0)	ω_e (cm^{-1})	D_e (units of mE_h)	R_e (units of a_0)	ω_e (cm^{-1})
$(1)^1\Sigma_g^+$	7.30	6.70	77.4	7.04	7.00	69.2
$(2)^1\Sigma_g^+$	6.93	6.70	76.0	6.55	7.44	69.9
$(3)^1\Sigma_g^+$	6.30	7.15	81.1	6.18	7.23	100.8
$(1)^1\Sigma_u^-$	6.49	7.05	75.4	6.79	7.44	79.8
$(2)^1\Sigma_u^-$	6.24	7.20	79.2	6.34	7.27	76.4
$(1)^3\Sigma_g^-$	12.07	5.55	94.4	8.61	6.52	93.4
$(2)^3\Sigma_g^-$	6.27	7.20	77.8	7.38	7.32	94.9
$(1)^3\Sigma_u^+$	6.15	7.20	78.1	6.84	7.44	82.9
$(2)^3\Sigma_u^+$	5.77	7.15	72.7	5.35	7.38	74.8
$(3)^3\Sigma_u^+$	4.52	7.45	61.1	4.57	7.64	59.8
$(1)^1\Pi_g$	6.44	7.10	77.2	6.58	7.32	79.7
$(2)^1\Pi_g$	5.25	7.25	68.4	5.26	7.47	70.5
$(1)^1\Pi_u$	7.71	6.55	75.8	7.01	7.01	61.7
$(2)^1\Pi_u$	6.50	6.95	81.0	6.53	7.19	93.6
$(1)^3\Pi_g$	6.33	7.10	76.0	6.37	7.34	78.5
$(2)^3\Pi_g$	5.09	7.25	67.4	5.16	7.47	70.0
$(1)^3\Pi_u$	9.63	6.00	86.7	8.10	6.55	81.3
$(2)^3\Pi_u$	6.75	6.95	79.6	6.85	7.21	82.3
$(1)^1\Delta_g$	8.18	6.45	84.0	7.76	6.82	76.2
$(2)^1\Delta_g$	5.85	7.15	72.8	5.77	7.40	69.9
$(1)^1\Delta_u$	5.43	7.25	70.8	6.09	7.45	74.7
$(1)^3\Delta_g$	6.08	7.05	74.8	6.20	7.30	76.6
$(1)^3\Delta_u$	5.86	7.10	72.9	6.17	7.43	74.0
$(2)^3\Delta_u$	5.76	7.20	73.7	5.75	7.43	73.5
$(1)^1\Phi_g$	6.43	7.10	77.5	6.60	7.34	81.3
$(1)^1\Phi_u$	6.62	7.05	78.0	6.74	7.29	79.1
$(1)^3\Phi_g$	6.42	7.05	76.6	6.65	7.32	79.0
$(1)^3\Phi_u$	6.75	6.95	76.6	6.73	7.22	77.3
$(1)^1\Gamma_g$	6.46	7.20	78.8	6.69	7.46	73.2
$(1)^3\Gamma_u$	6.32	7.25	78.1	6.84	7.43	81.7

size consistency is observed in the numerical calculations. This deviation is not explained by symmetry breaking in the underlying CASSCF calculations. In order to obtain a physical description of the long-range interaction, we combine the NEVPT2 results at short-range with a long-range model. The quadrupole-quadrupole coupling strength and the dispersion coefficients are determined from complete active space calculations and atomic polarizabilities at the TD-DFT level, respectively. This yields a physical description of the 30 molecular states correlating to the $^2D_g + {}^2D_g$ dissociation limit, and inferred spectroscopic parameters which are in reasonable agreement with known MRCI results. In addition to adiabatic PECs, diabatic potentials are presented, which are employed in scattering calculations in the companion paper [35].

ACKNOWLEDGMENTS

The authors thank Renzo Cimiraglia for sharing his implementation of the QD-NEVPT2 program, as well as for critically analyzing our results. X.C. acknowledges support by National Science Foundation Award No. PHY-0855676. Ad van der Avoird is acknowledged for carefully reading the manuscript.

APPENDIX: ASYMPTOTIC WAVE FUNCTIONS

The theoretical asymptotic wave functions are the eigenvectors of the asymptotic interaction, i.e., the quadrupole-quadrupole coupling [32]. Apart from a single scaling factor, this interaction is known analytically, and its angular dependence is given by the $k_A = k_B = 2$, $k_{AB} = 4$ part of the tensorial expansion Eq. (3). The scaling does not affect the eigenvectors, which are found by diagonalizing the matrix representation of this interaction. We use a body-fixed basis of Russel-Saunders coupled states, $|L_A\Lambda_A\rangle|L_B\Lambda_B\rangle$. That is, we take the internuclear axis parallel to the z axis such that we have

$$C_{kq}(\hat{\boldsymbol{R}}) = \delta_{q0} = \begin{cases} 1 & \text{if } q = 0 \\ 0 & \text{if } q \neq 0 \end{cases}. \tag{A1}$$

Then, the matrix elements are given by

$$\begin{aligned} &\langle L_A\Lambda_A|\langle L_B\Lambda_B|[T_2(L_A)\otimes T_2(L_B)]_0^{(4)}|L_A\Lambda'_A\rangle|L_B\Lambda'_B\rangle \\ &\quad = 5(-1)^{L_A-\Lambda_A+L_B-\Lambda_B}\sum_q \langle 2q2-q|40\rangle \\ &\qquad \times \begin{pmatrix} L_A & 2 & L_A \\ -\Lambda_A & q & \Lambda'_A \end{pmatrix}\begin{pmatrix} L_B & 2 & L_B \\ -\Lambda_B & -q & \Lambda'_B \end{pmatrix}. \end{aligned} \tag{A2}$$

Numerical diagonalization yields the theoretical eigenstates in the basis $\{|L_A M_A\rangle|L_B M_B\rangle\}$.

We denote the eigenfunctions, which are labeled with the $\Lambda = \Lambda_A + \Lambda_B$ quantum number, as $|\chi_{c,\Lambda}\rangle$, where c labels the eigenstates. The contribution of atomic states $|L_A\Lambda_A\rangle|L_B\Lambda_B\rangle$ to this molecular state is given by

$$w^{(c,\Lambda)}_{\Lambda_A,\Lambda_B} = |\langle\chi_{c,\Lambda}|L_A\Lambda_A\rangle|L_B\Lambda_B\rangle|^2. \tag{A3}$$

This weight is used in the counterpoise procedure for the BSSE correction of the potential energy for state $|\chi_{c,\Lambda}\rangle$. The BSSE-corrected adiabatic potential is calculated as

$$V_{c,\Lambda}(R) = E^{(AB)}_{c,\Lambda}(R) - \sum_{\Lambda_A,\Lambda_B} w^{(c,\Lambda)}_{\Lambda_A,\Lambda_B}\left[E^{(A)}_{\Lambda_A}(R) + E^{(B)}_{\Lambda_B}(R)\right], \tag{A4}$$

where $E^{(A)}_{\Lambda_A}$ and $E^{(AB)}_{c,\Lambda}$ are the monomer and dimer energies, evaluated in the dimer basis, with the subscripts denoting the electronic state.

In order to be able to compare the theoretical asymptotic wave functions to the CASSCF results, both results should be expressed in the same basis. In MOLPRO, the state is expanded in a basis of Slater determinants with different occupation of the active orbitals. For simplicity, we assume the atoms are described by a pure $[\mathrm{Ar}]4s^2 3d^1$ configuration and ignore all contributions of other configurations. The basis of Slater determinants is properly antisymmetrized with respect to the interchange of any two electrons, in contrast to the states $|L_A\Lambda_A\rangle|L_B\Lambda_B\rangle$, where each electron is associated with either atom A or B. This difference may be accounted for by explicitly antisymmetrizing the long-range-theoretical result. Furthermore, the angular part of the one-electron functions is treated differently, as real spherical harmonics are used in MOLPRO. They are related to the usual spherical harmonics through

$$C_{l0,c} = C_{l0}, \tag{A5}$$

and for $m > 0$

$$C_{lm,c} = \frac{1}{\sqrt{2}}[(-1)^m C_{lm} + C_{l-m}],$$
$$C_{lm,s} = \frac{-i}{\sqrt{2}}[(-1)^m C_{lm} - C_{l-m}]. \tag{A6}$$

Finally, these functions are adapted to D_{2h} symmetry as

$$C^{\pm}_{lm,c/s} = \frac{1}{2}\sqrt{2}(1 \pm \hat{i})C^{(A)}_{lm,c/s}$$
$$= \frac{1}{2}\sqrt{2}\left[C^{(A)}_{lm,c/s} \pm (-1)^l C^{(B)}_{lm,c/s}\right], \tag{A7}$$

where A,B denote the functions are centered at the respective atom.

These relations are used to express both states in the same basis. Before comparing the expansion coefficients, an arbitrary overall phase was fixed by requiring the scalar product of both states to be real and positive. Furthermore, we point out that the exclusion of all configurations other than $[\mathrm{Ar}]4s^2 3d^1$ leaves the CASSCF wave function unnormalized. Therefore, we have normalized the resulting CASSCF state, according to the norm of the CASSCF wave function of the separated atoms, where all configurations other than $[\mathrm{Ar}]4s^2 3d^1$ were excluded, as well.

[1] C. C. Bradley, C. A. Sackett, J. J. Tollett, and R. G. Hulet, Phys. Rev. Lett. **75**, 1687 (1995).
[2] J. B. Anderson, Ann. Rev. Phys. Chem. **14**, 85 (1995).
[3] K. B. Davis, M.-O. Mewes, M. R. Andrews, N. J. van Druten, D. S. Durfee, D. M. Kurn, and W. Ketterle, Phys. Rev. Lett. **75**, 3969 (1995).
[4] A. T. Nguyen, D. Budker, S. K. Lamoreaux, and J. R. Torgerson, Phys. Rev. A **69**, 022105 (2004).
[5] V. A. Dzuba, V. V. Flambaum, and M. V. Marchenko, Phys. Rev. A **68**, 022506 (2003).
[6] M. R. Tarbutt, J. J. Hudson, B. E. Sauer, and E. A. Hinds, Faraday Discuss. **142**, 37 (2009).
[7] H. L. Bethlem and W. Ubachs, Faraday Discuss. **142**, 25 (2009).
[8] T. Kraemer, M. Mark, P. Waldburger, J. G. Danzl, C. Chin, B. Engeser, A. D. Lange, K. Pilch, A. Jaakkola, H.-C. Nägerl *et al.*, Nature (London) **440**, 315 (2006).
[9] D. DeMille, Phys. Rev. Lett. **88**, 067901 (2002).
[10] B. L. Lev, E. R. Meyer, E. R. Hudson, B. C. Sawyer, J. L. Bohn, and J. Ye, Phys. Rev. A **74**, 061402 (2006).
[11] K. M. Jones, E. Tiesinga, P. D. Lett, and P. S. Julienne, Rev. Mod. Phys. **78**, 483 (2006).
[12] T. Köhler, K. Góral, and P. S. Julienne, Rev. Mod. Phys. **78**, 1311 (2006).
[13] N. Masuhara, J. M. Doyle, J. C. Sandber, D. Kleppner, T. J. Greytak, H. F. Hess, and G. P. Kochanski, Phys. Rev. Lett. **61**, 935 (1988).
[14] J. Söding, D. Guéry-Odelin, P. Desbiolles, G. Ferrari, and J. Dalibard, Phys. Rev. Lett. **80**, 1869 (1998).
[15] R. V. Krems, G. C. Groenenboom, and A. Dalgarno, J. Phys. Chem. A **108**, 8941 (2004).
[16] C. I. Hancox, S. C. Doret, M. T. Hummon, L. Luo, and J. M. Doyle, Nature (London) **431**, 281 (2004).
[17] J. G. E. Harris, S. V. Nguyen, S. C. Doret, W. Ketterle, and J. M. Doyle, Phys. Rev. Lett. **99**, 223201 (2007).
[18] R. V. Krems, J. Kłos, M. F. Rode, M. M. Szczesniak, G. Chałasinski, and A. Dalgarno, Phys. Rev. Lett. **94**, 013202 (2005).
[19] M.-J. Lu, K. S. Hardman, J. D. Weinstein, and B. Zygelman, Phys. Rev. A **77**, 060701 (2008).
[20] B. Zygelman and J. D. Weinstein, Phys. Rev. A **78**, 012705 (2008).
[21] C. B. Connolly, Y. S. Au, S. C. Doret, W. Ketterle, and J. M. Doyle, Phys. Rev. A **81**, 010702 (2010).
[22] A. Kalemos, I. G. Kaplan, and A. Mavridis, J. Chem. Phys. **132**, 024309 (2010).
[23] C. Camacho, H. A. Witek, and R. Cimiraglia, J. Chem. Phys. **132**, 244306 (2010).
[24] I. G. Kaplan and U. Miranda, AIP Advances **1**, 022108 (2011).
[25] A. A. Buchachenko, G. Chałasinski, and M. M. Szczesniak, J. Chem. Phys. **132**, 024312 (2010).
[26] T. Helgaker, P. Jørgensen, and J. Olsen, *Molecular Electronic Structure Theory* (Wiley, Chichester, 2000).

[27] C. Angeli, R. Cimiraglia, S. Evangelisti, T. Leininger, and J. P. Malrieu, J. Chem. Phys. **114**, 10252 (2001).
[28] C. Angeli, R. Cimiraglia, and J. Malrieu, J. Chem. Phys. **117**, 9138 (2002).
[29] C. Angeli, S. Evangelistia, R. Cimiraglia, and D. Maynau, J. Chem. Phys. **117**, 10525 (2002).
[30] C. Angeli, M. Pastore, and R. Cimiraglia, Theor. Chim. Acta **117**, 743 (2007).
[31] K. G. Dyall, J. Chem. Phys. **102**, 4909 (1995).
[32] G. C. Groenenboom, X. Chu, and R. V. Krems, J. Chem. Phys. **126**, 204306 (2007).
[33] X. Chu and A. Dalgarno, J. Chem. Phys. **121**, 4083 (2004).
[34] X. Chu and A. Dalgarno, Adv. Atom. Mol. Optical Phys. **51**, 83 (2005).
[35] T. Karman and G. C. Groenenboom, following paper, Phys. Rev. A **90**, 052702 (2014).
[36] B. Zygelman, A. Dalgarno, and R. D. Sharma, Phys. Rev. A **49**, 2587 (1994).
[37] V. Kokoouline, R. Santra, and C. H. Greene, Phys. Rev. Lett. **90**, 253201 (2003).
[38] R. Santra and C. H. Greene, Phys. Rev. A **67**, 062713 (2003).
[39] S. H. Lipoff and D. R. Herschbach, Mol. Phys. **108**, 1133 (2010).
[40] S. Kotochigova and A. Petrov, Phys. Chem. Chem. Phys. **13**, 19165 (2011).
[41] X. Chu, A. Dalgarno, and G. C. Groenenboom, Phys. Rev. A **72**, 032703 (2005).
[42] N. Babalabanov and K. Peterson, J. Chem. Phys. **123**, 064107 (2005).
[43] H.-J. Werner and W. Meyer, J. Chem. Phys. **73**, 2342 (1980).
[44] H.-J. Werner and W. Meyer, J. Chem. Phys. **74**, 5794 (1981).
[45] H.-J. Werner and P. J. Knowles, J. Chem. Phys. **82**, 5053 (1985).
[46] P. J. Knowles and H.-J. Werner, Chem. Phys. Lett. **115**, 259 (1985).
[47] H.-J. Werner, AIP Advances **69**, 1 (1987).
[48] H.-J. Werner *et al.*, http://www.molpro.net.
[49] R. Lindh, U. Ryu, and B. Liu, J. Chem. Phys. **95**, 5889 (1991).
[50] F. B. van Duijneveldt, J. G. C. M. van Duijneveldt-van der Rijdt, and J. H. van Lenthe, Chem. Rev. **94**, 1873 (1994).
[51] S. F. Boys and F. Bernardi, Mol. Phys. **19**, 553 (1970).
[52] M. H. Alexander, J. Chem. Phys. **99**, 6014 (1993).
[53] J. Kłos, G. Chałasiński, M. M. Szczęśniak, and H.-J. Werner, J. Chem. Phys. **115**, 3085 (2001).
[54] J. Kłos, M. F. Rode, G. Chałasiński, and M. M. Szczęśniak, Eur. Phys. J. D **31**, 429 (2004).
[55] M. C. G. N. van Vroonhoven and G. C. Groenenboom, J. Chem. Phys. **116**, 1954 (2002).
[56] H. Köppel, W. Domcke, and L. S. Cederbaum, Adv. Chem. Phys. **57**, 59 (1984).
[57] J. Kłos, J. Chem. Phys. **123**, 024308 (2005).
[58] K. T. Tang and J. P. Toennies, J. Chem. Phys. **80**, 3726 (1984).